

# High energy power-law tail in X-ray binaries spectrum and bulk Comptonization due to a conical outflow from a disk

Nagendra Kumar\*

Department of Physics, Indian Institute of Science, Bangalore 560012, India

## Abstract

X-ray binaries (XRBs) often exhibit a high energy power-law tail (X-ray) and these tails can be generated by the bulk Comptonization (BMC) process with a free-fall bulk region onto the compact object. We frequently observe a radio emission (which is generated by a synchrotron-emitting outflowing electrons) from the XRBs. We aim to study the high energy power-law tail in BMC process by an outflowing medium. We mainly consider a collimated and conical (of opening angle  $\theta_b$  with axis perpendicular to the accretion disk) outflow for a BMC process. We simulate the bulk Comptonized spectra by using a Monte Carlo scheme. Out of two possible conical outflow directions i) along the surface of the cone, ii) inside the conic region, we find that a) the randomness of outflow directions increases with  $\theta_b$ , b) the emergent spectra have power-law tail (of photon index  $\Gamma > 2$  and with high energy cut-off  $E_c > 200$  keV) only for  $\theta_b$  greater than  $\sim 30$  degree, while for a collimated or a conical outflow ( $\theta_b < 30$  degree) these power-law tail can be only generated when it is also found in thermal Comptonized spectra (i.e., at sufficiently high medium temperature). We compare the GRS 1915+105 spectra for two classes  $\chi$  and  $\gamma$ , for this the outflow speed is highly relativistic and the relevancy of wind parameters suggest that wind must be occurred at inner region of the accretion disk, so consistent with inner disk radio emission.

Key Words: stars: black holes – stars: neutron – X-rays: binaries – individual: GRS 1915+105 – radiation mechanisms: thermal

## 1 Introduction

Black hole (BH) low mass X-ray binaries (LMXBs) frequently change their X-ray spectral states particularly power-law dominated low intense hard (LH) state to blackbody dominated high intense soft (HS) state via outburst, which again settles down to the LH state. During the spectral state transition, sometimes a very high intense power-law dominated (VHS) state with photon index  $\Gamma$  greater than 2.4 is observed without an exponential high energy cut-off ( $E_c$ ) and generally referred as a steep power law (SPL) state (for review see, Done et al., 2007, McClintock & Remillard, 2006). High energy power-law tail ( $\Gamma > 2.0$ ) is observed in both state LH and HS, which extends up to  $\geq 200$  keV [e.g., McConnell et al., 2002, Motta et al., 2009, Titarchuk & Shaposhnikov, 2010] and also detected in neutron star (NS) LMXBs [e.g., Revnivtsev et al., 2014].

The low energy (2-100 keV) power-law component has been believed due to a thermal comptonization (TC) of a disk photons, but for the high energy power-law tail ( $E_c > 200$  keV) a modified version of TC has been invoked. Example, Done & Kubota [2006] assumed that the disk and Comptonizing medium are energetically coupled to each other [see also, Kubota & Done, 2016]; in hybrid model a hybrid electron distribution (thermal + non-thermal [power law]) has been considered [Coppi, 1999, Gierliński et al., 1999] and in bulk Comptonization (BMC) model electrons are in a free-fall converging flow of spherically accreted plasma into BH (Titarchuk et al., 1997, and for NS e.g., Farinelli et al., 2009).

In BMC framework, for a spherically diverging outflow, Laurent & Titarchuk [2007] had noticed only down-scattering of the soft spectrum, i.e., no high energy power-law tail [see also, Ghosh et al., 2010, Psaltis, 2001]. Outflow observe in all spectral state of LMXBs, e.g., jet outflow is in LH & SPL state and wind outflow is in HS state [e.g., Degenaar et al., 2016, Díaz Trigo & Boirin, 2016, Fender & Belloni, 2012, Miller et al., 2016, Ponti et al., 2012]. Wind and jet can be exist simultaneously e.g., in LMXBs [Drapeau et al., 2017, Homan et al., 2016, Tetarenko et al., 2018], in active galactic nuclei [e.g., Tombesi et al., 2014], and morphologically, in some systems the wind outflow geometry has been inferred to be a conical shape [e.g., Degenaar et al., 2016, Knigge et al.,

---

\*E-mail:nagendra.bhu@gmail.com

1995, Tombesi et al., 2015]. Moreover, we observe radio emission in all spectral state of LMXBs, the radio flux of HS is 10 to 1000 times fainter than the VHS radio flux, the jet power of VHS is positively correlated with peak X-ray luminosity of HS, and it is believe that the radio emission of VHS is due to the synchrotron process by outflowing relativistic electron near to the compact object on accretion disk [e.g., Fender et al., 2004, 1999, Fender & Hendry, 2000, Fender et al., 2009, Fender & Kuulkers, 2001, Munro et al., 2001, Rushton et al., 2012, Zhang & Yu, 2015]. Recently, Motta et al. [2018] have emphasized that the radio-loud/quiet nature of BH LMXBs can be an inclination effect, i.e., the low inclination source is radio loud and vice versa but it will also depends on opening angle of outflow e.g., V404 Cyg is a high inclination source and radio-loud. In this paper, we motivate to study the high energy power-law tail by BMC process in outflow with a conical and collimated outflow. We compute the spectra by using a Monte Carlo method, and we find that when the outflow is a conical type (i.e., at any scattering point P the electron outflow/ bulk direction is any one of the directions inside the cone of opening angle  $\theta_b$  at P) then the soft photons can get upscattered and the emergent spectra have a power-law component.

## 2 Monte Carlo Method

In bulk Comptonization, the photons are upscattered due to both thermal and bulk motions of the electrons and it was initially formulated by Blandford & Payne [1981a,b]. In other words, BMC process employs two components of electron velocity simultaneously, in generalized case of BMC process, it may be possible that no one velocity component corresponds to the bulk motion [e.g., Kaufman & Blaes, 2016, and references therein], in that case the spectra can be computed by implementing the Monte Carlo methods. We are interested to study the BMC process by conical outflow and the outflow direction is not unique at any point in conical outflow, so for present purpose we develop a Monte Carlo (MC) scheme for a generalized BMC process (however for rest of paper we will still refer it as a BMC process). The mean free path of the photons  $\lambda$  in motive medium will get increased in comparison to the static medium and it is taken into account [e.g., Sazonov & Sunyaev, 2000]. The algorithm for MC code is similar to that of Kumar & Misra [2016] for a thermal Comptonization part and for the bulk (outflow) motion effect we adopt a similar to that discussed by Laurent & Titarchuk [1999], Niedźwiecki & Zdziarski [2006] by neglecting general relativistic effects.

The average energy exchange per scattering for a monochromatic photon of energy  $E$  in corona having temperature  $kT_e$  and a bulk flow with constant speed  $u_b$  [Titarchuk et al., 1997] is  $\Delta E = \Delta E_{TH} + \left( \frac{4u_b}{c\tau} + \frac{(u_b/c)^2}{3} \right) \frac{E}{m_e c^2}$ . Here,  $\Delta E_{TH} = (4kT_e - E) \frac{E}{m_e c^2}$  is for thermal Comptonization i.e.,  $u_b = 0$ ,  $\tau$  is the optical depth of the scattering medium,  $m_e$  is the rest mass of the electron and  $k$  is Boltzmann constant. If the bulk direction is taken to be random, like thermal motion, and if the  $\Delta E$  is same for a given sets of  $kT_e$  and  $u_b$  then the emergent spectra for these sets would be same for a given average scattering number ( $\langle N_{sc} \rangle$ ).

Particularly, we check the MC code by comparing the simulated bulk Comptonized spectrum to thermal Comptonized one for those parameters sets which have same  $\Delta E$ , for example, the sets ( $kT_e = 3$  keV,  $u_b = 0$ ) for TC and ( $kT_e = 2$  keV,  $u_b = 0.0766c$ ) for BMC; here we neglect the term  $\frac{4u_b}{c\tau}$ . The emergent spectra for both sets are identical for either single, or multiple scattering or Wien peak spectrum (i.e. for large  $\langle N_{sc} \rangle \sim 500$ ) which are shown by curve 1, 2 and 3 in Fig. 1 respectively.

## 3 Emergent spectrum from Outflow geometry

We assume that the outflow occurs on the accretion disk and for an outflow region we consider a torus surrounding the compact object, which has a rectangular cross-section [e.g., Kumar & Misra, 2016]. The meridional cut of the torus is shown in Fig. 2. We fix a global spherical polar coordinate ( $r, \theta, \phi$ ) at the center of the torus. Without loss of generality we assume, the torus exists only above the equatorial plane and when the scattered photons cross the equatorial plane, these photons will get absorbed. We assume that the optical depth is along the vertical direction so the electron density in the torus is  $n_e = \frac{\tau}{L\sigma_T}$ , where  $\sigma_T$  is Thompson cross-section and  $L$  is the vertical height of the torus. The seed photon source is a blackbody at temperature  $kT_b$ , which emits vertically from the equatorial plane of the accretion disk. We take the seed source inside the outflow region, depending upon size of the torus two extreme possibility can be possible. In first case the major fraction of scattered photons escape from top of the torus while for 2nd case, from outer boundary of the torus. Without loss of generality to extract the general picture we consider a first case and we take  $w = 10$  km,  $L = 1$  km.

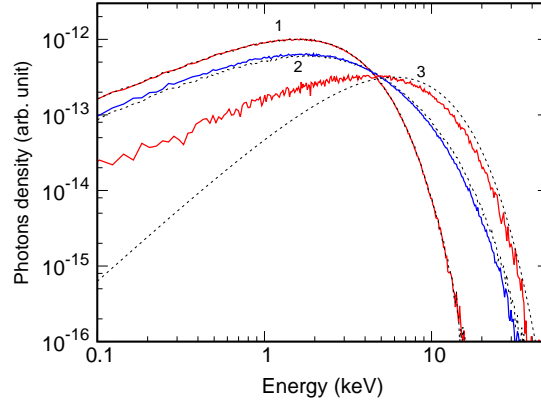


Figure 1: Spectra comparing Monte Carlo results. The solid lines are for bulk Comptonization ( $kT_e = 2$  keV,  $u_b=0.0766c$ ) and dashed lines are for thermal Comptonization ( $kT_e = 3$  keV,  $u_b=0.0$ ). The curves 1, 2, and 3 are for single scattering, multiple scattering ( $\langle N_{sc} \rangle \sim 46$ ), and Wien peak ( $\langle N_{sc} \rangle > 500$ ).

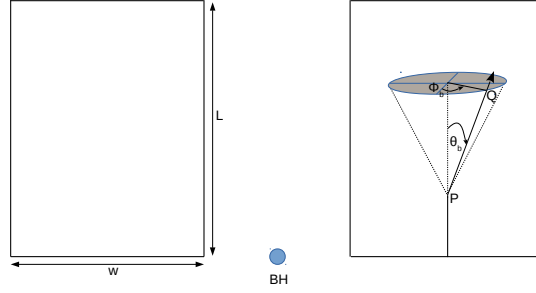


Figure 2: Meridional cut of a rectangular torus surrounding the BH to study the outflow motion. The conic shaded region is for a possible conical outflow direction at the scattering point P. Here, PQ is one of outflow direction ( $\theta_b$ ,  $\phi_b$ ); w is width and L is height of the torus.

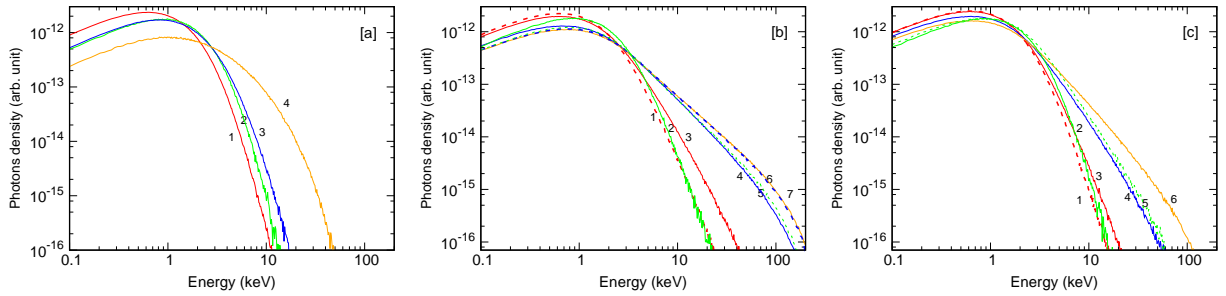


Figure 3: The simulated emerged spectra for different outflow geometry. The left is for collimated outflow, while middle and right panels are for case I and II in conical outflow respectively. In left panel the curves 1,2,3 and 4 are for  $\theta_b = 0$  (outflow), 180 (inflow), 90 and 90 degree. In middle and right panel the curves 1,2,3,4,5, and 6 are for  $\theta_b = 20, 160, 30, 60, 110$ , and 90 degree respectively. In middle panel the curve 7 (dashed) is for 95 degree. The spectral parameters for all curves are  $kT_e=3.0$  keV,  $kT_b=0.5$  keV,  $\tau = 3$  and  $u_b = 0.45$  c except for 4th curve of left panel where  $\tau = 15$  and  $u_b = 0.65$  c.

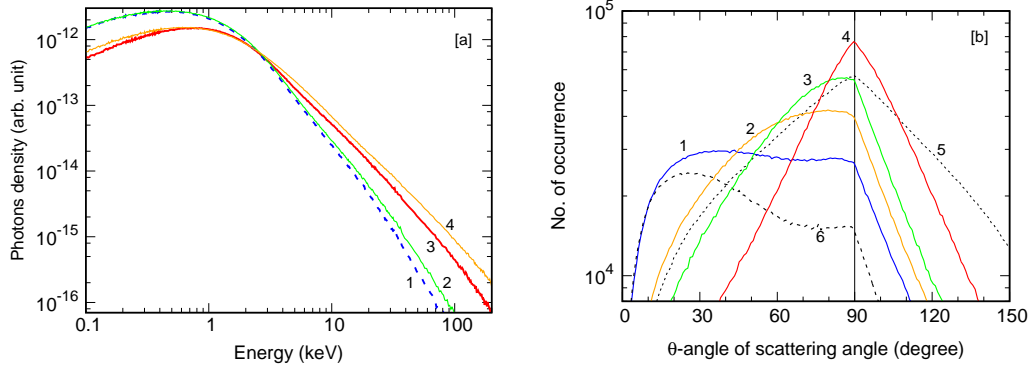


Figure 4: The left panel is for an emergent spectra for a high medium temperature ( $kT_e = 30$  keV). The curve 3 is for a spectra of thermal dominated case ( $(u_b/c)^2 \ll 3kT_e/(m_e c^2)$ ), while others are for bulk dominated case,  $u_b = 0.75c$ . The curve 1 is for collimated outflow of  $\theta_b = 15$  degree, and the curves 2, 4 are for conical outflow of  $\theta_b = 15$ , and 45 degree respectively. The right panel is for scattering angle distribution. Curves 1, 2, 3, 4 are for conical outflow of  $\theta_b = 15, 45, 60, 90$  degree respectively and  $u_b = 0.75c$ , and the curve 6 is for  $\theta_b = 15$  degree and  $u_b = 0.85c$ . The curve 5 is for thermal dominated case. The rest parameters are  $kT_b = 0.5$  keV and  $\tau = 1$ .

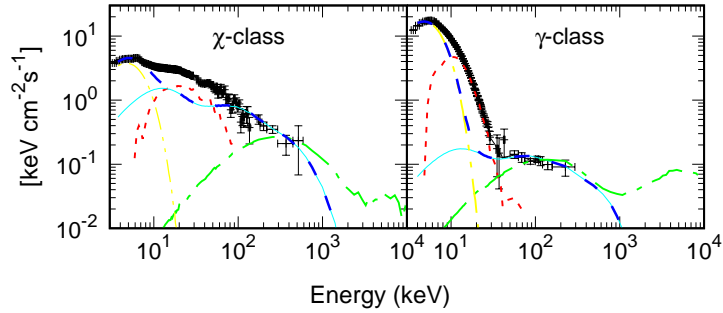


Figure 5: Comparison of the  $\chi$  (left panel)  $\gamma$  (right panel) class of GRS 1915+105 with the bulk Comptonization model, here the data points are taken from Zdziarski et al. [2001]. The two-dotted-dashed, solid, dashed, and dotted curves are for blackbody (BB), bulk Comptonization (BMC), BB + BMC, and residual (data - (BB + BMC)) components respectively. Here,  $\theta_b = 30$  degree,  $u_b = 0.95c$ ,  $kT_e = 3$  keV,  $kT_b = 1.2$  keV and  $\tau = 2.0$  ( $\chi$ -class) = 2.8 ( $\gamma$ -class). Dotted-dashed curve is for BMC component when  $u_b = 0.998c$  and the other components are not shown here.

Table 1: Sets of (outflow speed  $u_b$ , optical depth  $\tau$ ) and high energy cut-off  $E_c$  of bulk dominated BMC spectra of photon index  $\Gamma \sim 2.5$  in conical outflow.

$kT_e$	$(u_b, \tau), E_{cut}^a$ (MeV) when		
	$\theta_b=30^\circ$	$\theta_b=45^\circ$	$\theta_b=60^\circ$
3keV	(0.8c, 5.2), 0.7	(0.72c, 2.0), 0.6	(0.6c, 1.9), 0.4
	(0.85c, 4.2), 0.8	(0.85c, 1.2), 0.8	(0.7c, 1.2), 0.6
30keV	(0.8c, 2.8), 1.1	(0.85c, 0.8), 1.2	(0.7c, 0.6), 0.8
	(0.7c, 2.6), 0.8	(0.7c, 0.9), 0.8	(0.6c, 0.7), 0.6

a: one can notice,  $E_{cut}$  increases with  $u_b$  (or  $kT_e$ ) for given  $kT_e$  (or  $u_b$ ) and for fixed value of  $E_{cut}$  and  $\Gamma$ ,  $u_b$  and  $\tau$  get decrease by increasing  $kT_e$ .

For outflow geometry we consider a conical outflow of opening angle  $\theta_b$  with the axis perpendicular to the equatorial plane. We assigned the outflow direction locally by the same global coordinate with  $(\theta_b, \phi_b)$ , as shown in Fig. 2, so the  $\theta_b < 90$  degree corresponds to the outflow,  $\theta_b > 90$  degree is for inflow and  $\theta_b = 90$  degree is neither a inflow nor outflow but a flow which is parallel to the disk plane. We are first interested to study a collimated outflow. With the definition of a conical outflow, the collimated outflow is determined from  $\theta_b = \text{constant}$ , and  $\phi_b \equiv \phi$ -angle of a scattering point in a global coordinate. We select the collimated outflow direction away from the compact object. The emergent spectra for collimated outflow are shown in Fig. 3a. We do not find a high energy power-law tail in the collimated outflow even in the extreme condition like curve 4 of Fig. 3a at low medium temperature ( $kT_e = 3$  keV). Our results are consistent with Janiuk et al. [2000] that the multiple scattered spectra in inflow ( $\theta_b = 180$  degree) is red-shifted from single scattered spectra.

We have computed the thermal Comptonized spectra (or thermal dominated BMC spectra i.e.,  $(u_b/c)^2 \ll 3kT_e/(m_e c^2)$ ) for large  $kT_e = 30$  keV. The power-law tail has been seen, as shown by the curve 3 in Fig. 4a also in curve 1, which is for a collimated outflow of  $\theta_b = 15$  degree,  $u_b = 0.75c$  (a bulk dominated BMC spectra), hence, in collimated outflow the power-law tail can be found for sufficiently large  $kT_e$ . The above results are consistent with Kylafis et al. [2014], where they described the power-law component in soft gamma-ray repeaters by BMC process with having a vertically downward bulk region onto the neutron star pole for a large  $kT_e$ . [see also Titarchuk et al., 2012, for a power-law component of gamma-ray burst spectrum].

Next we consider two different plausible cases of conical outflow geometry. In case I we simply consider, the outflow direction at scattering point P is in any one of directions on the surface of the cone from the vertex P, that is,  $\theta_b = \text{constant}$  and  $\phi_b$  varies from 0 to  $2\pi$ . While in case II the outflow direction can be any one of directions within the conical region so here  $\theta_b$  will vary from 0 to  $\theta_b = \text{constant}$ , and  $\phi$  will vary again from 0 to  $2\pi$ . We first study the variation of BMC spectra with opening angle for both cases, which is shown in Fig. 3b, c. We find, the photon index decreases with  $\theta_b$  for both cases and the spectrum of case I is harder than the case II. Further, we notice that to generate the power-law tails with  $E_c > 200$  keV and observed range of  $\Gamma (> 2)$ , the  $\theta_b$  should be greater than 30 degree and  $u_b > 0.4c$  for low  $kT_e$ . Evidently, the case II is more plausible for conical outflow. For simplicity to extract the general picture for BMC process in conical outflow we consider the case I. In Table 1, we list the few BMC parameters range, mainly  $(u_b, \tau)$  along with  $E_c$  for a typical photon index  $\sim 2.5$  for case I. We find, the high energy cut-off  $E_c$  increases with  $u_b$  for given  $kT_e$ .

In conical outflow for low  $kT_e$  we find, when  $\theta_b > 30$  degree then photons get upscattered and a power-law tail is observed in BMC spectra and for  $\theta_b < 30$  degree there is no power-law tail in spectra due to downscattering. We reexamine this by computing the spectra for large  $kT_e (= 30$  keV). For  $\theta_b < 30$  degree, the  $\Gamma$  will increase from thermal dominated one by increasing the outflow speed due to downscattering of the soft photons and contrary,  $\Gamma$  will decrease with  $u_b$  for  $\theta_b > 30$  degree, these are illustrated in Fig. 4a (it, downscattering of photons, is hold upto  $u_b \sim 0.99c$ ). Similarly, for a collimated outflow the  $\Gamma$  will increase with  $u_b$ . In Fig. 4b, the distribution of scattering angle (the angle between scattered and incident photon) has been shown for a conical outflow (case I) with four different outflow direction  $\theta_b = 15, 45, 60$  and  $90$  degree. It seems that the scattered photons are in the outflow direction of electron and it tends to be more along a outflow direction for a large value of  $u_b$ . In terms of the randomness, the outflow direction becomes more random as  $\theta_b$  is increased and it becomes completely random (like thermal ones, as shown by curve 5 in Fig. 4b) when  $\theta_b$  tends to 90 degree. As the collimated case in a conical outflow for  $\theta_b$  less than 30 degree, the power-law tails can be produced when the power-law tails are also produced in thermal dominated regime.

In Fig. 5 we compare qualitatively the observed  $\chi$  (LH) and  $\gamma$  (HS) class of GRS 1915+105 with bulk

Comptonized spectra at low medium temperature. The data points are taken from Zdziarski et al. [2001]. We compute black body (BB) and BMC component and we obtain the residual after subtracting these two components (BB+BMC) to the data points. Here, the X-ray spectrum is well described by three components BB, BMC and third components, residual, which may be arisen either due to a relativistic reflection spectra Ross & Fabian [2005] or due to TC component or both [e.g., Farinelli et al., 2009, Kubota & Done, 2016, McConnell et al., 2002, Revnivtsev et al., 2014]. To check the consistency of results, we compute the wind parameters like the mass outflow rate  $\dot{M}_{wind} = \Omega \mu m_p n_e R^2 u_b$  and the kinetic power of the wind  $L_{kin} = \dot{M}_{wind} c^2 \left( \frac{1}{\sqrt{1-(u_b/c)^2}} - 1 \right)$ , here  $\Omega$  is the covering factor,  $\mu$  is the mean atomic weight,  $m_p$  is the mass of the proton,  $R$  is the launching radius and  $n_e = \frac{\tau}{L \sigma_T}$  is electron density [Miller et al., 2016]. For outflow speed  $u_b = 0.95c$ ,  $\dot{M}_{wind} = 1.2 \times 10^{15}$ ,  $1.7 \times 10^{15}$  g/s; and  $L_{kin} = 2.2 \times 10^{39}$ ,  $3.1 \times 10^{39}$  erg/s are for  $\chi$  and  $\gamma$  class respectively. Here we consider the launching radius  $R = 10R_S$ ,  $R_S$  is Schwarzschild radius and mass of BH is  $10M_\odot$ . We also extract the wind parameters for higher  $u_b = 0.998c$  and large  $kT_e = 100$  keV (where  $\tau = 0.8$  and  $3.0$  for  $\chi$  and  $\gamma$  class respectively,  $E_{cut} \geq 10$  MeV). We find that the estimated kinetic power of the wind for both cases is 2 to 10 times larger than the corresponding luminosity ( $= 6.5 \times 10^{38}$ ,  $1.7 \times 10^{39}$  erg/s for  $\chi$  and  $\gamma$  class respectively, Zdziarski et al., 2001.) of both classes, the results are consistent with the radio emission which also believes to generate inner regions of the accretion disk.

## 4 Summary and Discussion

As it was noticed earlier that a spherically diverging outflow geometry is not a favourable ones to generate the high energy power-law tail by bulk Comptonization process, we investigate the different outflow geometry mainly a collimated and conical outflow from the accretion disk. We simulate the emergent BMC spectrum by a Monte Carlo scheme with considering, the seed photon source is on equatorial plane of the disk and inside the outflow region. For conical outflow, we consider two different outflow directions for electron, in case I it is in any one of the direction along the surface of the cone and in case II it is in any one of direction within the conic region.

The power-law tail with observed  $\Gamma$  and  $E_c$  can not be formed in collimated outflow, but it can form in conical outflow when  $\theta_b$  is greater than  $\sim 30$  degree for a low medium temperature. In conical outflow the outflow direction has many probable direction in each point of the medium, i.e., seemingly a turbulent flow. It is generally believed that an accretion flow is turbulent, so some gas can move outward which further accelerate to the infinity. Yuan et al. [2015] have shown a tangled trajectory of test particles in magnetohydrodynamics MHD simulation for accretion flow/ outflow. In conical outflow, we find that the randomness of the outflow direction is increased with increasing  $\theta_b$  and for  $\theta_b$  tends to 90 degree the outflow direction is completely random. In simplistic and systematic way the turbulent outflow behavior may study by the conical outflow (especially case II). In general we find, the emergent spectrum of case I is harder than the case II. The photon index of power-law component decreases with increasing  $\theta_b$ . For high  $kT_e$  ( $> 25$  keV), the power-law tail with observed  $\Gamma$  and  $E_c$  can be generated by thermal or bulk Comptonization process. In other words, for conical outflow of  $\theta_b < 30$  degree and for collimated outflow, the high-energies power-law tail would be also generated, when it will found in thermal dominated case.

Qualitatively, we match the observations and we need third components other than black body and bulk Comptonization components which may be arisen due to either thermal Comptonization or relativistic reflection or both. In Fig. 5 we match the both spectral state HS and LH for low medium temperature  $kT_e = 3$  keV (for  $E_{cut} \sim 1$  MeV). In LMXBs, the observationally inferred  $kT_e$  has wide range depending upon the spectral state [McConnell et al., 2002, Parker et al., 2016, Titarchuk et al., 2014, Zdziarski et al., 2001], so we fit the spectra (for  $E_{cut} \sim 1$  MeV) for higher  $kT_e = 50$  keV, and the respective  $u_b = 0.88c$  and  $\tau = 1.4$  and  $1.9$  are for  $\chi$  and  $\gamma$ -class respectively (for general results, see Table 1). Hence, for low or high  $kT_e$  our estimated outflow speed is highly relativistic. The estimated wind parameters especially the kinetic power of the wind suggest that wind will take place at the inner accretion disk, like radio emission. For such highly relativistic inner wind the acceleration mechanism can be a magnetic origin or thermal origin or combination of both [e.g., Chakravorty et al., 2016, de Gouveia dal Pino & Lazarian, 2005, Dexter et al., 2014, Higginbottom & Proga, 2015, Reynolds, 2012, Tchekhovskoy et al., 2011]. The highly relativistic inner wind implies a radio emission and we observe the radio emission in all spectral states. Also, the radio flux should be correlated with high energy tail flux, e.g., in case of GRS 1915+105 the radio flux of HS is 10-100 times fainter than LH/ VHS radio flux and the flux of high energy tail in HS state is 2-10 times lower than LH or VHS [Muno et al., 2001, Zdziarski et al., 2001]. Hence the presented model for high energy power-law tail by bulk Comptonization with outflowing medium is consistent to the observed variation of radio emission with spectral state of LMXBs. For a relativistic outflow speed, the scattered photons are mostly in outflow direction, so the high energies power-law tail would be a beam polarized,



in some system the polarization of power-law tail has been detected (e.g., Rodriguez et al., 2015, for crab pulsar e.g., Vadawale et al., 2017). In general the presented model spectra are degenerate over coronal temperature, outflow speed and opening angle of conical outflow, the degeneracy may be resolved, by studying the variation of disk black body temperature or the X-ray timing variability with spectral state of LMXBs, or by correlation study of the radio emission to high energy power-law tails (or radio-loud vs radio-quiet LMXBs) or by incorporating self-consistently an acceleration mechanism.

## Acknowledgement

Author is supported by University Grants Commission, New Delhi India through Dr. D.S. Kothari Post-Doctoral Fellowship (201718-PH/17-18/0013). Author acknowledges partial financial support from Indian Space Research Organisation (ISRO) with research Grant No. ISTC/PPH/BMP/0362. He wishes to thank Ranjeev Misra for valuable comments on this project and Banibrata Mukhopadhyay for their valuable suggestions and comments over the manuscript.

## References

- Blandford, R. D. & Payne, D. G. 1981a, MNRAS, 194, 1041
- Blandford, R. D. & Payne, D. G. 1981b, MNRAS, 194, 1033
- Chakravorty, S., Petrucci, P.-O., Ferreira, J., et al. 2016, A&A, 589, A119
- Coppi, P. S. 1999, in Astronomical Society of the Pacific Conference Series, Vol. 161, High Energy Processes in Accreting Black Holes, ed. J. Poutanen & R. Svensson, 375
- de Gouveia dal Pino, E. M. & Lazarian, A. 2005, A&A, 441, 845
- Degenaar, N., Altamirano, D., Parker, M., et al. 2016, MNRAS, 461, 4049
- Dexter, J., McKinney, J. C., Markoff, S., & Tchekhovskoy, A. 2014, MNRAS, 440, 2185
- Díaz Trigo, M. & Boirin, L. 2016, Astronomische Nachrichten, 337, 368
- Done, C., Gierliński, M., & Kubota, A. 2007, A&A Rev., 15, 1
- Done, C. & Kubota, A. 2006, MNRAS, 371, 1216
- Drappeau, S., Malzac, J., Coriat, M., et al. 2017, MNRAS, 466, 4272
- Farinelli, R., Paizis, A., Landi, R., & Titarchuk, L. 2009, A&A, 498, 509
- Fender, R. & Belloni, T. 2012, Science, 337, 540
- Fender, R. P., Belloni, T. M., & Gallo, E. 2004, MNRAS, 355, 1105
- Fender, R. P., Garrington, S. T., McKay, D. J., et al. 1999, MNRAS, 304, 865
- Fender, R. P. & Hendry, M. A. 2000, MNRAS, 317, 1
- Fender, R. P., Homan, J., & Belloni, T. M. 2009, MNRAS, 396, 1370
- Fender, R. P. & Kuulkers, E. 2001, MNRAS, 324, 923
- Ghosh, H., Garain, S. K., Chakrabarti, S. K., & Laurent, P. 2010, International Journal of Modern Physics D, 19, 607
- Gierliński, M., Zdziarski, A. A., Poutanen, J., et al. 1999, MNRAS, 309, 496
- Higginbottom, N. & Proga, D. 2015, ApJ, 807, 107
- Homan, J., Neilsen, J., Allen, J. L., et al. 2016, ApJ, 830, L5

Janiuk, A., Czerny, B., & Życki, P. T. 2000, *MNRAS*, 318, 180

Kaufman, J. & Blaes, O. M. 2016, *MNRAS*, 459, 1790

Knigge, C., Woods, J. A., & Drew, J. E. 1995, *MNRAS*, 273, 225

Kubota, A. & Done, C. 2016, *MNRAS*, 458, 4238

Kumar, N. & Misra, R. 2016, *MNRAS*, 461, 4146

Kylafis, N. D., Trümper, J. E., & Ertan, Ü. 2014, *A&A*, 562, A62

Laurent, P. & Titarchuk, L. 1999, *ApJ*, 511, 289

Laurent, P. & Titarchuk, L. 2007, *ApJ*, 656, 1056

McClintock, J. E. & Remillard, R. A. 2006, Black hole binaries (Lewin, W. H. G. and van der Klis, M.), 157–213

McConnell, M. L., Zdziarski, A. A., Bennett, K., et al. 2002, *ApJ*, 572, 984

Miller, J. M., Raymond, J., Fabian, A. C., et al. 2016, *ApJ*, 821, L9

Motta, S., Belloni, T., & Homan, J. 2009, *MNRAS*, 400, 1603

Motta, S. E., Casella, P., & Fender, R. P. 2018, *MNRAS*, 478, 5159

Muno, M. P., Remillard, R. A., Morgan, E. H., et al. 2001, *ApJ*, 556, 515

Niedźwiecki, A. & Zdziarski, A. A. 2006, *MNRAS*, 365, 606

Parker, M. L., Tomsick, J. A., Kennea, J. A., et al. 2016, *ApJ*, 821, L6

Ponti, G., Fender, R. P., Begelman, M. C., et al. 2012, *MNRAS*, 422, L11

Psaltis, D. 2001, *ApJ*, 555, 786

Revnivtsev, M. G., Tsygankov, S. S., Churazov, E. M., & Krivonos, R. A. 2014, *MNRAS*, 445, 1205

Reynolds, C. S. 2012, *ApJ*, 759, L15

Rodriguez, J., Grinberg, V., Laurent, P., et al. 2015, *ApJ*, 807, 17

Ross, R. R. & Fabian, A. C. 2005, *MNRAS*, 358, 211

Rushton, A., Miller-Jones, J. C. A., Campana, R., et al. 2012, *MNRAS*, 419, 3194

Sazonov, S. Y. & Sunyaev, R. A. 2000, *A&A*, 354, L53

Tchekhovskoy, A., Narayan, R., & McKinney, J. C. 2011, *MNRAS*, 418, L79

Tetarenko, B. E., Lasota, J.-P., Heinke, C. O., Dubus, G., & Sivakoff, G. R. 2018, *Nature*, 554, 69

Titarchuk, L., Farinelli, R., Frontera, F., & Amati, L. 2012, *ApJ*, 752, 116

Titarchuk, L., Mastichiadis, A., & Kylafis, N. D. 1997, *ApJ*, 487, 834

Titarchuk, L., Seifina, E., & Shrader, C. 2014, *ApJ*, 789, 98

Titarchuk, L. & Shaposhnikov, N. 2010, *ApJ*, 724, 1147

Tombesi, F., Meléndez, M., Veilleux, S., et al. 2015, *Nature*, 519, 436

Tombesi, F., Tazaki, F., Mushotzky, R. F., et al. 2014, *MNRAS*, 443, 2154

Vadawale, S. V., Chattopadhyay, T., Mithun, N. P. S., et al. 2017, *Nature Astronomy*, 1

Yuan, F., Gan, Z., Narayan, R., et al. 2015, *ApJ*, 804, 101

Zdziarski, A. A., Grove, J. E., Poutanen, J., Rao, A. R., & Vadawale, S. V. 2001, *ApJ*, 554, L45

Zhang, H. & Yu, W. 2015, *MNRAS*, 451, 1740